Biomech Model Mechanobiol (2011) 10:577–589
DOI 10.1007/s10237-010-0257-z

ORIGINAL PAPER

A multiphysics/multiscale 2D numerical simulation of scaffold-based cartilage regeneration under interstitial perfusion in a bioreactor

Riccardo Sacco · Paola Causin · Paolo Zunino · Manuela T. Raimondi

Received: 6 April 2010 / Accepted: 8 September 2010 / Published online: 24 September 2010

Abstract In vitro tissue engineering is investigated as a potential source of functional tissue constructs for cartilage repair, as well as a model system for controlled studies of cartilage development and function. Among the different kinds of devices for the cultivation of 3D cartilage cell colonies, we consider here polymeric scaffold-based perfusion bioreactors, where an interstitial fluid supplies nutrients and oxygen to the growing biomass. At the same time, the fluid-induced shear acts as a physiologically relevant stimulus for the metabolic activity of cells, provided that the shear stress level is appropriately tuned. In this complex environment, mathematical and computational modeling can help in the optimal design of the bioreactor configuration. In this perspective, we propose a computational model for the simulation of the biomass growth, under given inlet and geometrical conditions, where nutrient concentration, fluid dynamic field and cell growth are consistently coupled. The biomass growth model is calibrated with respect to the shear stress dependence on experimental data using a simplified short-time analysis in which the nutrient concentration and the fluid-induced shear stress are assumed constant in time and uniform in space. Volume averaging techniques are used to derive effective parameters that allow to upscale the microscopic structural properties to the macroscopic level. The biomass growth predictions obtained in this way are significant for long times of culture.

Keywords Tissue engineering · Artificial cartilage · Computational model · Multiphysics · Multiscale · Interstitial perfusion · Bioreactor · Fluid dynamics · Transport · Shear stress

The Author RS was partly supported by the GNCS–INdAM Research Funding Program 2010 "Modelli Computazionali per Problemi Multifisica/Multiscala in Presenza di Bio-Interfacce". The Author PC was supported by the Italian Research Funding Program PRIN 2007 "Modellistica numerica per il calcolo scientifico ed applicazioni avanzate". The Author PZ was supported by the European Research Council Advanced Grant "Mathcard, Mathematical Modelling and Simulation of the Cardiovascular System", Project ERC-2008-AdG 227058. The Author MTR was partly supported by the Italian Institute of Technology (IIT), Genoa, Italy.

R. Sacco
Dipartimento di Matematica "F. Brioschi", Politecnico di Milano, Piazza L. da Vinci, 32, 20133 Milano, Italy
e-mail: riccardo.sacco@polimi.it

P. Causin
Dipartimento di Matematica "F. Enriques", Università degli Studi di Milano, via Saldini, 50, 20133 Milano, Italy
e-mail: paola.causin@unimi.it

P. Zunino
MOX, Dipartimento di Matematica "F. Brioschi", Politecnico di Milano, Piazza L. da Vinci, 32, 20133 Milano, Italy
e-mail: paolo.zunino@polimi.it

M. T. Raimondi (✉)
LaBS, Dipartimento di Ingegneria Strutturale, Politecnico di Milano, Piazza L. da Vinci, 32, 20133 Milano, Italy
e-mail: manuela.raimondi@polimi.it

M. T. Raimondi
IRCCS Galeazzi Orthopaedic Institute, Milano, Italy

1 Introduction

A basic concept in the design of ex vivo tissue reconstruction is to provide a proper biophysical microenvironment to cells (Palsson and Bhatia 2004; Haj et al. 2005; Raimondi et al. 2006). In scaffold-based cartilage regeneration, a procedure for tissue growth based on interstitial flow of the culture medium ("direct" or "confined" perfusion) is found to be particularly effective, compared both to static

culture and surface perfusion, in preserving cell viability, promoting cell proliferation and up-regulating the synthesis of matrix proteins specific to cartilaginous tissue, such as collagens and glycosaminoglycan (GAG; Dunkelman et al. 1995; Pazzano et al. 2000; Davisson et al. 2002; Raimondi et al. 2002, 2004; Freyria et al. 2005). These beneficial effects are primarily related to an improved cell oxygenation and catabolite removal induced by interstitial convective flow in the internal regions of densely cell-populated constructs. Perfusion flow also exerts shear stresses on the cell surface, causing membrane stretch (Freed and Vunjak-Novakovic 2000; Guilak and Hung 2005); this mechanism is recognized to activate specific signaling pathways in articular cartilage cells provided that the shear stress level is appropriately tuned (Grodzinsky et al. 2000; Silver 2006). As a matter of fact, increasing the hydrodynamic shear level in cellular constructs is recognized to inhibit the synthesis of sulphated GAG (sGAG; Raimondi 2006) and of collagen type II (Raimondi et al. 2008), which are phenotypic markers of articular cartilage. The above considerations suggest that an efficient bioreactor should be able to provide the growing cells with the highest oxygenation level compatible with a moderate fluid-mechanical loading. Achieving such a balance is a difficult task, since there is a nonlinear interplay between the biophysical conditions at the microscopic pore scale and at the subcellular scale and the macroscopic design parameters of the bioreactor, such as the fluid velocity gradient or the pressure drop, which are directly related to input control parameters of the system (in our case, the inlet velocity of the perfusion fluid). Another difficulty is represented by the fact that the shear stress levels in the growing biomass are not easily accessible and data elaboration does not often allow to draw a clear rationale of the several occurring phenomena. In this scenario, mathematical and computational modeling can be profitably used to provide a supporting insight in the design of a bioreactor configuration, according to the following conceptual self–consistent methodological approach:

Task 1: simulation of the dynamical evolution of the environmental conditions to which cells are subjected (oxygenation level and shear stress distribution) as a function of the macroscopic control parameters.

Task 2: simulation of biomass growth under the action of the above computed biochemical and mechanical stimuli.

Task 3: introduction of a feedback mechanism, simulating the effect of the newly formed biomass on the environment (change of geometry, change of nutrient absorption).

The implementation of Task 1 requires to couple computational fluid dynamic (CFD) models with diffusion-advection-reaction equations for the nutrient. For this purpose, we use the Volume Averaging Method (VAM; Whitaker 1999) as a systematic technique to derive the Stokes-Brinkman equations for perfusion fluid flow and the diffusion-advection-reaction equation for nutrient mass transport, by upscaling to the macroscopic level (over a suitably defined averaging volume) the corresponding microscopic equations. The identification of "effective" parameters (effective diffusivity and effective hydraulic permeability) allows to characterize the system behavior at the macroscopic level by inheriting the properties of the microscale structure. In this crucial modeling step, all the available information (geometric, experimental, theoretical) on the sub-scale environment can be profitably used to enhance the accuracy of the upscaled model.

The implementation of Task 2 requires to develop, solve and validate models based on ordinary differential equations (ODE) and/or partial differential equations (PDE) to describe the evolution of the biomass under different stimulating or inhibitory factors. In the present article, we address this issue by the definition of a novel biomass growth model, which is a generalization of the one proposed in Galban and Locke (1999a,b) through the introduction of the dependence of the biomass growth parameters on the local or mean shear stress. To do this, we carry out a calibration procedure using experimentally measured data previously obtained from one of the Authors Raimondi (2006).

The implementation of Task 3 requires a detailed representation of the microscale phenomena and their effect on the variation of the porous structure of the scaffold. This problem is dealt with in the present article by the explicit characterization, using the VAM, of the effective nutrient diffusion coefficient and hydraulic permeability as a function of the spatially and time varying volume fraction occupied by the growing biomass (Hsu and Cheng 1990; Galban and Locke 1999b; Wood et al. 2002). An important improvement with respect to existing formulations (Chung et al. 2007) is the direct inclusion of measured data in the derivation of the model for the effective mass and fluid transport coefficients.

2 Theoretical model

Our computational model of the bioreactor structure shown in Fig. 1a encompasses three different phases, a polymeric porous scaffold, a perfusing fluid and a growing biomass, which coexist and evolve in space and time within the cellular construct shown in Fig. 1b. From now on, with the term "biomass" we denote the entire volume of biological matter resulting from cell proliferation and ECM synthesis. Let us denote by Ω the computational domain represented by the cellular construct in Fig. 1 and by ε_s, ε_f and ε_b the scaffold, fluid and biomass volume fractions, respectively. A schematic of the three considered phases is depicted in Fig. 1c, which also shows the averaging volume used for the application of the VAM. In order to set up the bioreactor model, we assume that the volume of the scaffold immersed

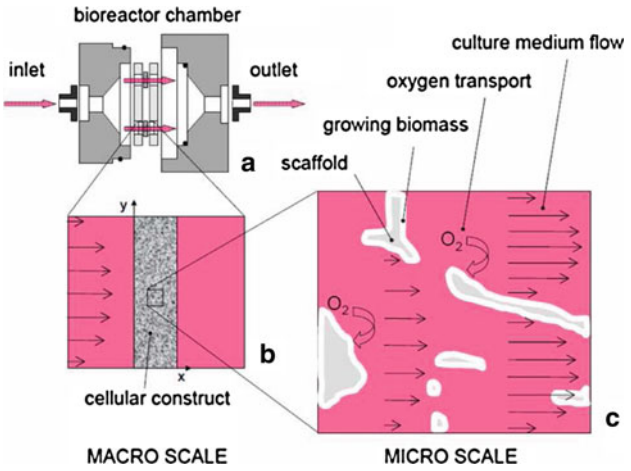

Fig. 1 Schematic of the modeled system: bioreactor chamber (**a**); macroscale representation of the cellular construct (**b**); details at the microscale level (**c**)

in the construct is time invariant, according to the fact that scaffold degradation is very slow compared to the overall culture time interval. This assumption implies that ε_s is a given constant quantity. Instead, the biomass volume varies with culture time, while consequently the fluid volume is modified in order to satisfy, at each spatial position $\mathbf{x} \in \Omega$ and at each time t the following constraint

$$\varepsilon_s + \varepsilon_f(\mathbf{x}, t) + \varepsilon_b(\mathbf{x}, t) = 1. \tag{1}$$

2.1 Biomass growth model

The increase in the biomass volume fraction can be derived starting from the mass conservation principle. This approach can be equivalently applied at different spatial scales. On one side, if the control volume is the entire scaffold, then the biomass volume fraction that is obtained is a single macroscopic value. On the other side, a pointwise mass balance and a corresponding governing equation can be obtained starting from an infinitesimal control volume centered around the generic point $\mathbf{x} \in \Omega$. Mass conservation allows us to state that biomass growth is governed by the evolution equation

$$\frac{\mathrm{d}\varepsilon_\mathrm{b}}{\mathrm{d}t} = (r_\mathrm{g} - r_\mathrm{d})\varepsilon_b = r_\mathrm{b}\varepsilon_b, \tag{2}$$

where r_d is the death rate accounting for the physiological cell apoptosis, r_g is a growth regulation factor and r_b is the net growth rate. Following Galban and Locke (1999a,b), in order to model r_g, we use the Monod growth kinetics modified by Contois in (1959)

$$r_\mathrm{g}(\varepsilon_b, c) = \frac{k_\mathrm{g} c}{k_\mathrm{s}\rho_\mathrm{b}\varepsilon_b + c}, \tag{3}$$

where c is the nutrient (oxygen) concentration, ρ_b is a reference biomass density, k_g is the maximum specific growth rate and k_s is a dimensionless parameter representing the Contois saturation constant. Observe that the evolution Eq. 2 is valid in the limit of small cell volume fractions, which is the case of the problem at hand. Should cell crowding effects be kept into account, a logistic–type law would be a more appropriate choice (see Lemon and King 2007). In Galban and Locke (1999a,b), the model parameter k_g is adjusted to fit experimental data obtained for different scaffold thicknesses in static culture conditions. As an established biomass growth model accounting for biomechanical stimuli is not yet present in the literature, we propose to modify relation (3) in such a way that k_g is a function of the shear stress state τ experienced by the cells

$$r_\mathrm{g}(\varepsilon_b, c, \tau; \boldsymbol{\xi}) = \frac{k_\mathrm{g}(\tau; \boldsymbol{\xi})c}{k_\mathrm{s}\rho_\mathrm{b}\varepsilon_b + c}, \tag{4}$$

where $\boldsymbol{\xi}$ denotes a set of unknown parameters to be determined by means of a calibration procedure based on experimental data.

2.2 Flow of the culture medium

We derive a macroscopic description of interstitial fluid flow perfusion throughout the scaffold porous matrix, using the following assumptions:

1. low perfusion regimes. This allows us to neglect inertial terms in the momentum balance equation;
2. the scaffold and biomass are rigid and impermeable to the fluid. This allows us to treat the fluid problem as a homogenized biphasic system (fluid and solid phases).

Applying the VAM over the averaging volume of Fig. 1c yields the following macroscopic Stokes equation system with Brinkman correction (Hsu and Cheng 1990; Wood and Whitaker 1998)

$$\begin{aligned} &\nabla \cdot \mathbf{v} = 0, \\ &\nabla p = -\mu\varepsilon_f K^{-1}(\varepsilon_f)\mathbf{v} + \mu\triangle\mathbf{v}, \end{aligned} \tag{5}$$

where μ is the dynamic viscosity of the culture medium, $\mathbf{v}$ is the Darcy velocity, p is the fluid pressure and K is the effective hydraulic permeability. An established closure relation expressing K as a function of the space and time dependent fluid volume fraction ε_f (related to the solid volume fraction by Eq. 1 is provided by the Carman-Kozeny equation (Bear 1972; Hsu and Cheng 1990; Wood and Whitaker 1998)

$$K(\varepsilon_f) = K_\mathrm{p}\frac{\varepsilon_f^3}{(1-\varepsilon_f)^2}, \tag{6}$$

where the Kozeny constant K_p is a reference permeability to be later specified.

2.3 Oxygen mass transport

Applying again the VAM over the averaging volume of Fig. 1c, and neglecting accumulation terms, yields the following mass conservation law in advective-diffusive-reactive form for the volume averaged oxygen concentration, c, in the homogenized phase

$$\nabla \cdot (-D\nabla c + \mathbf{v}c) + R(c) = 0, \tag{7}$$

where $c = \varepsilon_s c_\mathrm{s} + \varepsilon_f c_\mathrm{f} + \varepsilon_b c_\mathrm{b}$, and c_f, c_b are the volume averaged oxygen concentrations in the fluid and biomass phases, respectively, c_s is the negligible oxygen concentration inside the scaffold, $\mathbf{v}$ is the fluid velocity predicted by (5), D is the macroscopic diffusion coefficient, to be later discussed, and R is the biomass oxygen volumetric consumption rate, which is assumed to be a function of the local oxygen concentration according to the Michaelis–Menten kinetics

$$R(c) = \frac{R_\mathrm{m} c}{K_\mathrm{m} + c}\varepsilon_b, \tag{8}$$

R_m and K_m being the maximal consumption rate and the half saturation constant, respectively.

2.4 The complete mathematical model

Gathering together all the previously introduced differential sub-systems yields the following model for tissue engineering simulation:
find the porous medium velocity $\mathbf{v} = \mathbf{v}(\mathbf{x}, t)$ and pressure $p = p(\mathbf{x}, t)$, the nutrient concentration $c = c(\mathbf{x}, t)$ and the biomass volume fraction $\varepsilon_b = \varepsilon_b(\mathbf{x}, t)$, such that, for all $\mathbf{x} \in \Omega, t \in (0, T]$, we have

$$\nabla \cdot \mathbf{v} = 0, \tag{9a}$$
$$\nabla p = -\mu \varepsilon_f K^{-1}(\varepsilon_f)\mathbf{v} + \mu \triangle \mathbf{v}, \tag{9b}$$
$$\nabla \cdot (-D\nabla c + \mathbf{v}c) + R(c) = 0, \tag{9c}$$
$$\frac{d\varepsilon_b}{dt} = r_\mathrm{b}(\varepsilon_b, c, \tau)\varepsilon_b, \tag{9d}$$
$$\varepsilon_s + \varepsilon_b + \varepsilon_f = 1, \tag{9e}$$

supplied with the initial and boundary conditions specified later for each test case and with the appropriate definitions for K, R and r_b.

3 Methods

In order to close system (9), we proceed integrating two approaches: calibration on experimental data to determine $\boldsymbol{\xi}$ and K_p and computation of the effective oxygen diffusivity D using the VAM.

3.1 Experimental set-up for model calibration

We consider the bioreactor system described in Raimondi et al. (2006) and consisting of a bioreactor chamber in which chondrocyte-seeded cellular constructs are fixed on sterile discs, 1 mm in thickness, made of a biodegradable polyestherurethane foam with average porosity 77% (Cioffi et al. 2006). The constructs had their periphery sealed and were cultured under interstitial perfusion of the culture medium (refer to Fig. 1a for the chamber configuration). Four independent culture chambers were mounted in parallel; culture conditions were identical in each chamber, except for the construct diameter, equal to 2, 3, 4, or 7 mm, respectively. Keeping constant the inlet flow rate for each scaffold yields four different bioreactor configurations, each one being characterized by a given mean inlet velocity v_i, $i = 1, \ldots 4$. In Ref. Raimondi et al. (2006), CFD simulations are carried out on the uncellularised scaffold pore geometry in order to determine the median shear stress τ_i on the wall surfaces. Such shear stress is assumed to be representative of the actual biomechanical stimulus acting on the cell membrane for low biomass volume fractions. This assumption is common also to other computational studies performing a CFD simulation at the pore scale level (Cioffi et al. 2008; Lesman et al. 2010). Table 1 lists the values of v_i and τ_i, as well as the labels used to identify the four bioreactor configurations. Our calibration procedure is based on the complementary information provided in Fig. 4a and b of Raimondi et al. (2006), where the DNA and sGAG contents measured at $t = T = 15$ culture days are reported for each of the four culture conditions A, B, C, and D as a function of i, $i = 1, \ldots, 4$. From these data, it is possible to extract the cellular and ECM volume fractions, denoted by $\varepsilon^m_{\mathrm{c,i}}$ and $\varepsilon^m_{\mathrm{ECM,i}}$, corresponding to the discrete values τ_i and reported as well in Table 1. Noting that $\varepsilon^m_{\mathrm{b,i}} = \varepsilon^m_{\mathrm{c,i}} + \varepsilon^m_{\mathrm{ECM,i}}$, we obtain the pairs of data $(\tau_i, \varepsilon^m_{\mathrm{b,i}})$, $i = 1, \ldots, 4$.

3.1.1 Calibration of r_b

Assumptions In order to determine the set of parameters $\boldsymbol{\xi}$ entering the definition of the growth rate (4), we consider a short culture time $T = 15$ days. In this working condition, Eq. 9d can be regarded as the mathematical model for the time evolution of the average value of the biomass over the whole construct upon assuming space uniform and time-invariant control variables c and τ. These latter hypotheses are legitimate due to the following considerations:

1. the cell volume fraction is small. As a result of that, the oxygen consumption is negligible, which implies that the inlet concentration c_0 (saturation concentration in the fluid) can be used as a representative value for c;

Table 1 Scaffold configurations for model calibration (from Raimondi et al. (2006))

Scaffold diameter [cm]	Label	Index i	Inlet velocity v_i [cm/s]	Median shear stress τ_i [mPa]	Cell volume fraction	ECM volume fraction
0.2	A	1	0.884	56	0.0343	0.0366
0.3	B	2	0.393	25	0.0216	0.0231
0.4	C	3	0.221	14	0.0164	0.0187
0.7	D	4	0.072	4.6	0.0094	0.0125

2. the biomass volume fraction is small. As a result of that, the biomass does not yet significantly influence the fluid dynamics shear stresses on the scaffold walls. As a consequence, the median shear stress computed in Raimondi et al. (2006) by CFD models applied to the uncellularised scaffold can be used as a representative value for τ.

Under the above assumptions, the biomass growth is uncoupled from nutrient transport and tissue perfusion and can be solved independently. We consider a linear dependence of k_g on the shear stress, i.e.

$$k_g = k_{g0}(\alpha + \beta\tau), \tag{10}$$

where k_{g0} is the maximum growth rate in static conditions and α, β are the unknown fitting parameters of our model. Then, letting $\boldsymbol{\xi} = [\alpha, \beta]$, the vector $\boldsymbol{\xi}_{\text{fit}}$ that best fits in the least square sense the measured values of biomass volume is the solution of the following minimization problem

$$\boldsymbol{\xi}_{\text{fit}} = \underset{\boldsymbol{\xi}\in\mathbf{R}^2}{\text{argmin}} \sum_{i=1}^{4} (\varepsilon_b(T, c, \tau_i; \boldsymbol{\xi}) - \varepsilon_{\text{b,i}}^m)^2, \tag{11}$$

where, for a given function $f = f(x)$, the expression $\underset{x\in\mathbf{R}}{\text{argmin}}\, f(x)$ denotes the set of values of x for which $f(x)$ attains its minimum value.

Calibration of the cell growth model is carried out by solving Eq.2 with $k_{g0} = 5.8\times10^{-6}\text{s}^{-1}$ (corresponding to an average cell division time of 2 days), $k_s = 4.2 \times 10^{-3}$ (obtained using the standard Monod kinetics at equilibrium and normalizing the result to the initial value of the biomass fraction as done in Contois (1959) and an apoptosis rate $r_d = 3.85 \times 10^{-7}\text{s}^{-1}$ [corresponding to an average cell lifetime of 30 days (Galban and Locke 1999b)]. The initial value of the biomass is set equal to 0.02145 (see Sect. 4 for an extensive discussion of this choice). Using relation (4) into (2), the best fit parameters computed by solving Eq. 11 up to a tolerance of 10^{-5} are $\alpha = 0.8761$ and $\beta = 0.1045$. These results yield in Eq. 10 an amplification factor of the maximum growth rate of about 7 in correspondence of $\tau = \tau_4$. The small reduction of the value of k_g in static conditions ($\tau = 0$) should be ascribed to the fact that no experimental data are available for the fitting procedure in this situation. Figure 2 (top)

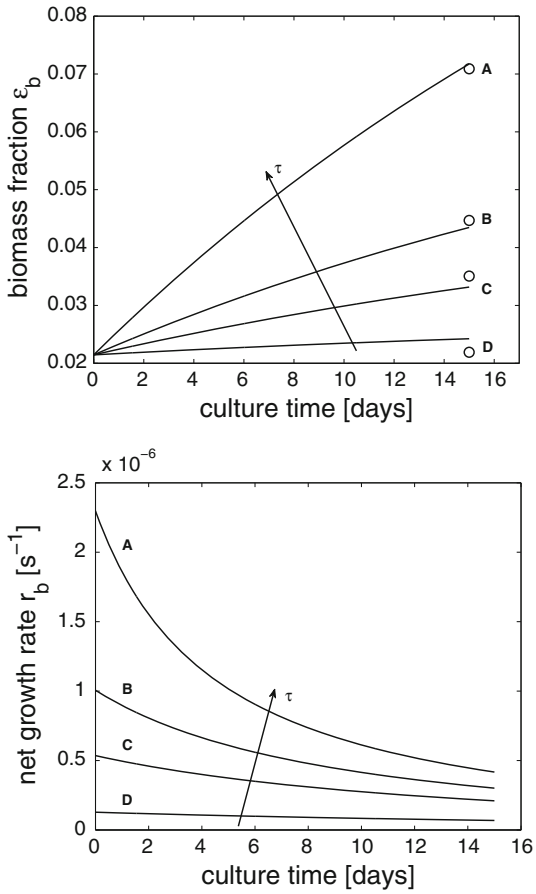

Fig. 2 Biomass volume fraction ε_b (*top*) and cell growth rate r_b (*bottom*) as a function of culture time. The *circles* denote experimental data as from Raimondi et al. (2006). The plots are obtained from the short-time model by solving Eq. 2, with the coefficients given in relation (4) and using the best fit parameters solution of Eq. 11

shows the computed biomass volume fraction as a function of culture time superposed with the experimentally measured quantities at $t = T = 15$ days (denoted by circles), while Fig. 2 (bottom) shows the biomass growth rate as a function of culture time as given by Eq. 4.

3.1.2 Calibration of K_p

In order to characterize the reference value of the hydraulic permeability K_p, the interstitial perfusion model must be

complemented with a definition of the expression of shear stress to be used in the context of VAM averaged equations. Under the assumption of low perfusion regimes, a commonly used model is an adaptation of the Darcy-Carman-Kozeny formula proposed in Wang and Tarbell (2000) to the case of a variable permeability

$$\tau(\varepsilon_b, |\mathbf{v}|; K_\mathrm{p}) = \frac{\mu|\mathbf{v}|}{\sqrt{K(\varepsilon_f)}} = \frac{\mu|\mathbf{v}|}{\sqrt{K(1-\varepsilon_s-\varepsilon_b)}}. \tag{12}$$

The above formula connects in an almost linear fashion the variation of the average shear stresses on the porous matrix walls to the average filtration velocity, as expected in these flow regimes. Moreover, the formula establishes a dependence of the stress on the actual biomass fraction. In order to characterize the Kozeny permeability K_p required to compute the effective hydraulic permeability given by Eq. 6, we use again a least square fitting between the values predicted by Eq. 12 by setting $\varepsilon_b = 0$ and $|\mathbf{v}|_i = v_i$, where $v_i, i = 1, \ldots, 4$ are the inlet velocities listed in Table 1. More precisely, we aim to find

$$K_{\mathrm{p,fit}} = \underset{K_\mathrm{p}\in\mathbf{R}}{\operatorname{argmin}} \sum_{i=1}^{4} \left(\tau(0, |\mathbf{v}|_i; K_\mathrm{p}) - \tau_i\right)^2,$$

τ_i, $i = 1, \ldots, 4$ being the median (pore-scale) shear stress computed in Raimondi et al. (2006) and reported in Table 1. The best fit value is $K_{\mathrm{p,fit}} = 1.97 \times 10^{-7}\mathrm{cm}^2$, which produces an extremely accurate fitting, the corresponding residual being of the order of 10^{-10}. The functions $\tau(\varepsilon_b, |\mathbf{v}|_i)$ obtained from relation (12) using the optimal value of $K_{\mathrm{p,fit}}$ are plotted in Fig. 3 in correspondence of $|\mathbf{v}|_i = v_i, i = 1, \ldots, 4$, showing that the shear stress is an increasing function of the biomass fraction, consistently with the fact that hydraulic resistance increases with cell proliferation. This analysis is particularly interesting in our case, because it provides an indication of the range of construct porosities where the present model can be considered to be reliable according to experimental validation. Indeed, it suggests that for long time cultures, where the biomass volume fraction is expected to grow significantly, only experiments with moderate inlet velocity, i.e. values C, D of Table 1, would correspond to shear stresses in the range where the present biomass growth model has been validated.

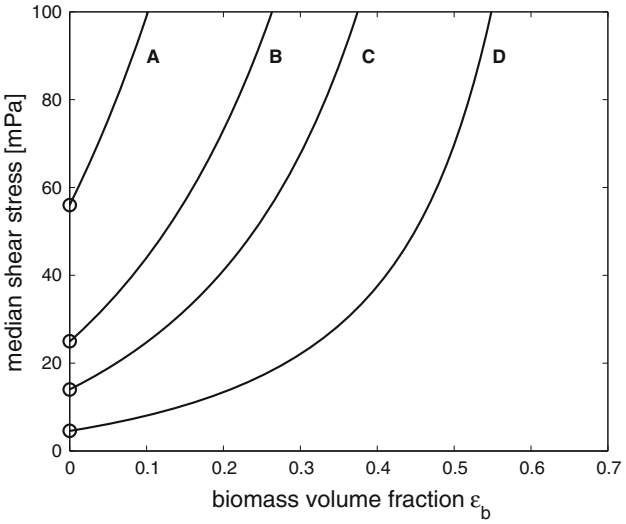

Fig. 3 Plot of the increase of shear stresses induced by biomass volume fraction growth. Each curve corresponds to a different value of the average velocity, equal to the inlet velocities A, B, C, D of Table 1, from *top* to *bottom*. The reference median shear stress values of Table 1 are highlighted with circle markers on the y axis

3.2 Effective oxygen diffusion coefficient

The multiphase structure of a cellular construct featuring three phases, fluid, biomass and solid scaffold, makes the determination of the effective oxygen diffusivity particularly challenging. As a matter of fact, a microscopic porosity relative to the scaffold structure, whose characteristic scale lies within the range of microns, coexists with a nanoscale porosity, which corresponds to the interstices between the fibers of the extracellular matrix. A comprehensive theory that allows to quantify in a simple manner the averaged diffusion properties of such complex material is not available yet. Different approaches exist for each specific scale: a first class of approaches includes models for the diffusion properties of continuum mixtures, such as solutions of polymers into a solvent (Masaro and Zhu 1999), and the concept of porosity is to be interpreted at the molecular scale. A second class of approaches has been developed in the framework of the VAM for geophysics, with application to discrete materials such as sands, gravels, soils (Whitaker 1999) and the concept of porosity is instead to be interpreted at the microscopic scale. Since in our tissue engineering problem we deal with relatively low biomass fractions, the role of ECM to hinder oxygen diffusion at the nanoscale can be neglected so that the porosity of the homogenized construct is assumed to be that of the sole microscale scaffold structure. Removing this restriction requires a (nontrivial) generalization of the present model to the case where cells and ECM are considered as independent phases. The following assumptions allow to reduce the complex system at hand to a simpler one, for which the effective diffusivity can be easily determined:

1. The main obstacle to free diffusion of dissolved molecules, such as oxygen, is the presence of the scaffold. The scaffold matrix is made of rigid walls impermeable to oxygen. This is equivalent to assuming that the oxygen diffusivity into the scaffold is negligible. This also allows us to conclude that the oxygen concentration into the scaffold is vanishing.

2. The oxygen diffusivity in the fluid phase is almost equivalent to the one into an agglomerate of cells, see Palsson and Bhatia (2004). We notice that this property would not be valid for molecules considerably larger than oxygen, such as glucose, for which the cell membrane represents an obstacle to diffusion.

Owing to the above assumptions, we can consider a biphasic system made of a "fluid-equivalent phase" (culture medium + biomass) and a solid phase (scaffold). In the fluid equivalent phase, we have the concentration $c_{\mathrm{fb}} = \varepsilon_{\mathrm{f}} c_{\mathrm{f}} + \varepsilon_{\mathrm{b}} c_b$, and, since $c_s = 0$, then $c \equiv c_{\mathrm{fb}}$, so that the diffusive flux in the biphasic system is

$$\mathbf{j} = -D\nabla c = -D_{\mathrm{fb}} \nabla c_{\mathrm{fb}}, \tag{13}$$

where D_{fb} is the effective diffusivity of the "fluid-equivalent phase" average concentration.

Let us denote by D'_{f} and D'_{b} the diffusivity of oxygen into a medium composed by either pure fluid or pure biomass, respectively. Assumption 2. implies that $D'_{\mathrm{f}} = D'_{\mathrm{b}}$ and that this value is also equal to the diffusivity D'_{fb} in a mixture of the twos. We now use Maxwell's model (Maxwell 1881; Wood et al. 2002) to find a closure relation for the diffusive flux into a biphasic system characterized by the scaffold with null diffusivity and by a "fluid-equivalent phase" with diffusivity equal to D'_{fb}

$$\frac{D_{\mathrm{fb}}}{D'_{\mathrm{fb}}} = M\left(\varepsilon_{\mathrm{fb}}, \kappa_{\mathrm{fb}}\right), \quad \kappa_{\mathrm{fb}} = k_{\mathrm{eq}} \frac{D'_s}{D'_{\mathrm{fb}}}$$

where

$$M(\varepsilon, \kappa) = \frac{2\kappa - \varepsilon(\kappa - 1)}{2 + \varepsilon(\kappa - 1)}$$

denotes Maxwell's formula (Maxwell 1881) in the case of an array of cylinders and k_{eq} is a suitable equilibrium constant, see Wood et al. (2002). Notice that the value of k_{eq} is irrelevant for us, since we assume that oxygen does not diffuse into the scaffold, so that $\kappa_{\mathrm{fb}} = 0$ for any possible finite value of k_{eq}. Combining the previous expressions, we obtain

$$\frac{D_{\mathrm{fb}}}{D'_{\mathrm{f}}} = \frac{2(1 - \varepsilon_s)}{2 + \varepsilon_s}$$

where the oxygen diffusivity D'_{f} in the pure fluid phase can be easily determined by measurements. We also notice that, in this specific case, the effective diffusivity coefficient, $D = D_{\mathrm{fb}}$, only depends on the scaffold volume fraction ε_s. This is a direct consequence of the assumption that the nutrient diffuses equivalently in the fluid and in the biomass.

4 Results

System (9) is discretized as outlined in Sect. 6.2 and numerical simulations are carried out within the Matlab software environment. The geometry of the computational domain is shown in Fig. 4, where $W = 1$ mm is the scaffold thickness and H is the scaffold diameter, chosen as in Table 1 for the different configurations. Moreover, $\mathbf{n}$ is the outward unit normal vector, $\mathbf{j}$ is the diffusive flux for the concentration field defined in (13) and $\mathbf{T} = 2\mu\boldsymbol{\varepsilon}(\mathbf{v}) - p\mathrm{Id}$ is the Stokes stress tensor, where $\boldsymbol{\varepsilon}(\mathbf{v})$ and Id denote the rate–of–strain tensor of the velocity field and the identity matrix, respectively. The inlet velocity field is a plug flow of modulus v_{in} (see Table 1). Numerical simulations (not reported here) carried out adding prior to the scaffold inlet section a sufficiently long tract of clear fluid in which Navier–Stokes equations have been solved, demonstrated that the computed fluid profile at the entrance of the porous section can be reasonably approximated by a constant velocity field. This choice is also coherent with the inlet boundary conditions prescribed by other authors (see, e.g., Cioffi et al. 2008; Lesman et al. 2010). The initial biomass volume fraction is computed from the prescribed total number N_{cells} of seeded cells used in Raimondi et al. (2006), supposing that at $t = 0$ the biomass is constituted only by cells. Cells can be seeded uniformly in the scaffold or be unevenly distributed. In the first case, denoting by $V_{\mathrm{cell}} = \frac{4}{3}\pi(d_{\mathrm{cell}}/2)^3$ the volume of the single cell, d_{cell} being the cell diameter, and by $V_{\mathrm{scaff}} = \pi(H/2)^2 W$ the scaffold volume, the initial volume fraction of cells can be straightforwardly computed as $\varepsilon_{\mathrm{b}}^0 = N_{\mathrm{cells}} \frac{V_{\mathrm{cell}}}{V_{\mathrm{scaff}}} = 0.02145$. The second case is discussed in detail later in the section. In the numerical simulations, only experimental scaffold configurations C and D are considered, in accordance with the previously drawn conclusions that the calibration of the full model is valid only for moderate median shear stresses. The values of the model parameters are listed in Table 2.

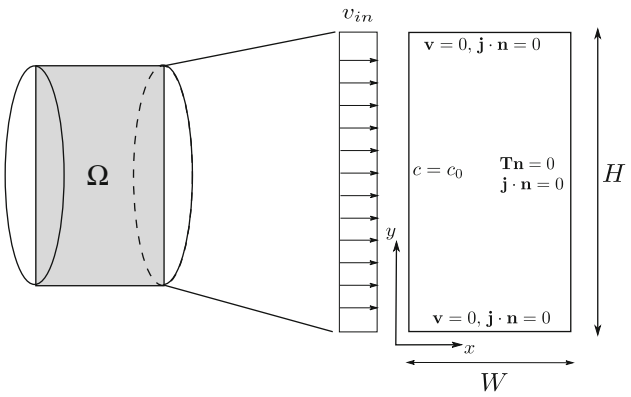

Fig. 4 Geometry of the computational domain and boundary conditions for the numerical simulations using the PDE/ODE model (9)

Table 2 Numerical values of the model parameters used in the computer simulations

Parameter	Dimension	Definition	Value	Ref.
c_0	[g/cm^3]	culture medium inlet O_2 concentration	6.4×10^{-6}	Palsson and Bhatia (2004)
D_f	[cm^2/s]	O_2 diffusivity in H_2O and biomass at 37°C	2.1×10^{-5}	Palsson and Bhatia (2004)
N_{cells}	[ ]	number of seeded cells	8×10^4	Raimondi et al. (2006)
d_{cell}	[mm]	diameter of the cell	8×10^{-3}	Raimondi et al. (2006)
ε_s	[ ]	scaffold volume fraction	0.23	Raimondi et al. (2006)
k_d	[1/s]	cell death rate	$1/(30 \times 24 \times 3600)$	Chung et al. (2007)
k_{g0}	[1/s]	maximum specific cell growth rate	$1/(2 \times 24 \times 3600)$	Palsson and Bhatia (2004)
k_s	[ ]	Contois cell saturation constant	4.2×10^{-3}	
μ	[g/(cm s)]	culture medium dynamic viscosity at 37°C	8.26×10^{-3}	Raimondi et al. (2002)
ρ_b	[g/cm^3]	reference biomass density	1	
R_m	[g/(cm^{3}s)]	O_2 maximal consumption rate	3.9×10^{-8}	Cioffi et al. (2008)
K_m	[g/cm^3]	O_2 half saturation constant	3.2×10^{-6}	Palsson and Bhatia (2004)

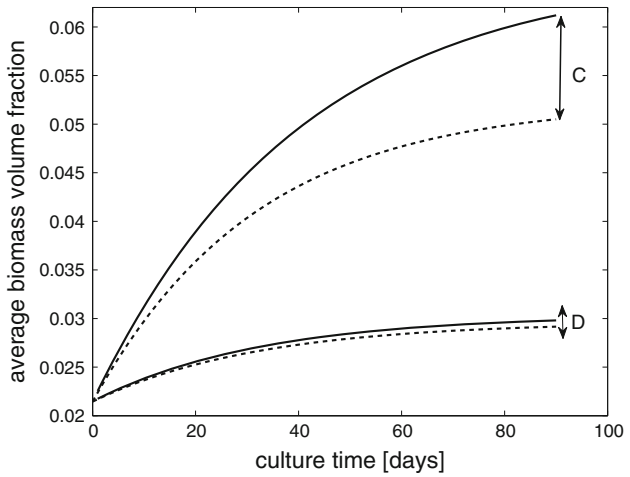

Fig. 5 Comparison between average biomass fraction predictions as a function of culture time obtained using different computational models. *Dashed lines* refer to the ODE model (2), while *solid lines* refer to the PDE/ODE model (9)

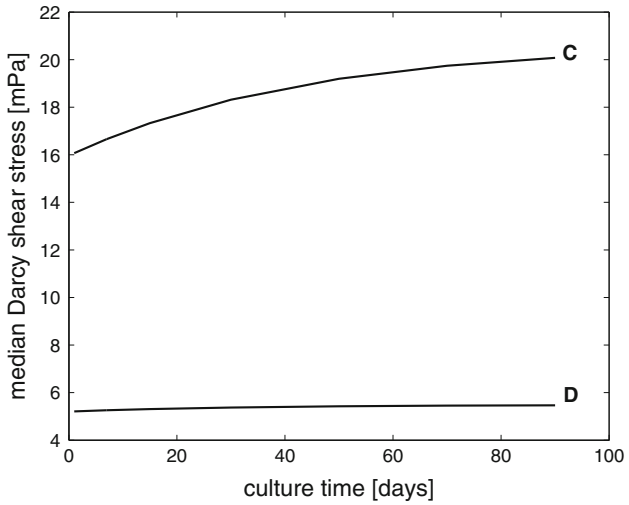

Fig. 6 Median Darcy stresses as a function of culture time for different scaffold configurations and computed by using the PDE/ODE model (9)

The first set of results refers to uniform seeding conditions. Figure 5 illustrates the comparison between predictions of the average biomass volume fraction (defined as the mean integral value of $\varepsilon_b(\mathbf{x}, t)$ over the scaffold area at each time t) obtained by running the sole ODE model (2) (dashed lines) and the full PDE/ODE model (9) (solid lines) up to a final culture time of $T = 90$ days. The discrepancy between the two models is related to the effect of the shear stresses, which are higher in the fully coupled model predictions with respect to the fixed value considered in the simple ODE model, because of the variation of permeability caused by the increasing biomass. Observe that shear stress and biomass production are tightly connected in a positive feedback loop, since a decrease in permeability due to biomass production leads to higher local shear stresses and, as a consequence, to higher biomass growth. Moreover, in the present case, discrepancies are more significant in scaffold C, because the inlet velocity in this configuration is higher than in scaffold D. This leads, since the very start of the culture process, to a general higher level of shear stresses in the scaffold, a higher growth rate and consequently a higher biomass production. Figure 6 shows the median Darcy stresses obtained by the PDE/ODE model as a function of culture time. Figure 7 shows for scaffold C the statistical distribution of the shear stresses evaluated in each element of the computational mesh. At advanced cell growth stages, as expected, the trend is a higher level of shear stresses throughout the whole domain. Moreover, a narrower distribution of the values is observed, in accordance with the results of Lesman et al. (2010). Figures 8 and 9 refer again to the scaffold configuration C, and show the snapshots of the spatial distribution, at various culture times, of the normalized oxygen concentration field and the biomass volume fraction (sampled at $y = H/2$).

The second set of results aims to investigate the effects of a nonuniform initial seeding of cells in the scaffold. To this purpose, we keep constant the total number of cells as

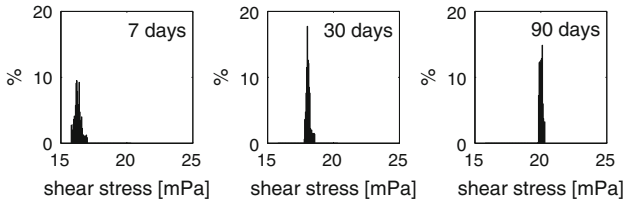

Fig. 7 Shear stress distributions at different times of culture for scaffold C

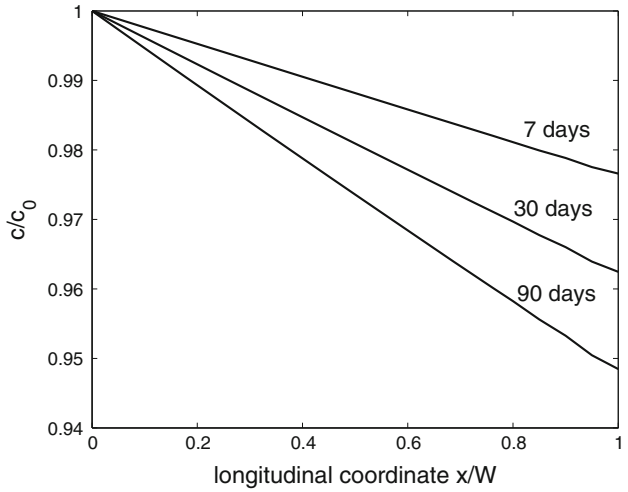

Fig. 8 Oxygen concentration (normalized to the inlet concentration c_0) at different culture times computed by using the PDE/ODE model (9). The x axis represents the dimensionless coordinate along the scaffold thickness

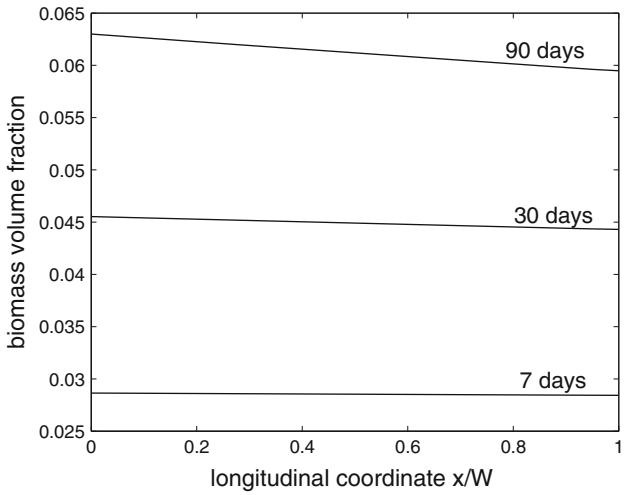

Fig. 9 Average biomass volume fraction at different culture times computed by using the PDE/ODE model (9). The x axis represents the dimensionless coordinate along the scaffold thickness

indicated in Table 2, while we allow the density of seeding to be a function of the spatial position inside the scaffold domain, so that also the initial biomass volume fraction is a function of the spatial position. In particular, we suppose

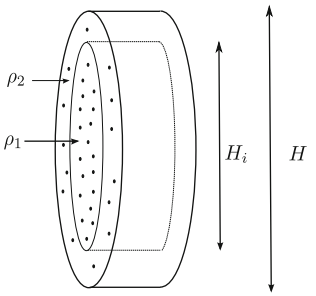

Fig. 10 Geometry and notation for the nonuniform seeding case study

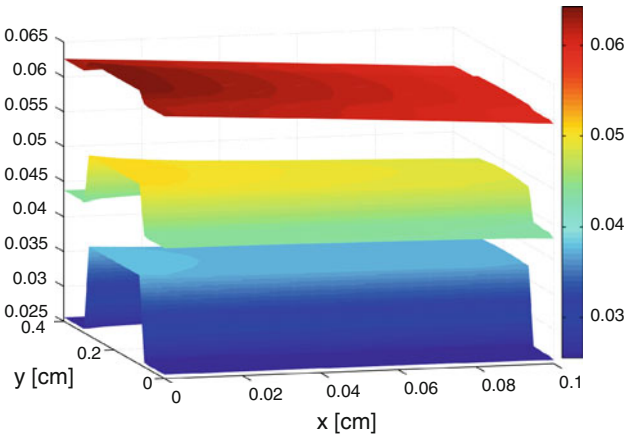

Fig. 11 Spatial distribution of the biomass volume fraction at $t = 7, 30, 90$ days of culture (from *bottom* to *top*) under nonuniform seeding conditions. The seeding density in the inner region is two times greater than the seeding density in the uniform seeding case

to have a certain seeding density ρ_1 in a cylindrical central region of diameter H_i of the 3D scaffold and a different seeding density ρ_2 in the remaining surrounding toroidal region (see Fig. 10).

The two densities are related by the convex combination

$$\frac{\rho_1}{\rho_{\text{seed}}}\xi^2 + \frac{\rho_2}{\rho_{\text{seed}}}(1-\xi^2) = 1,$$

where $\xi = H_i/H$ and $\rho_{\text{seed}} = N_{\text{cells}}/V_{\text{scaff}}$ is the cell density in the uniform seeding case. We set $\xi = 0.5$ and consider the scaffold configuration C. Then we carry out a first set of simulations choosing $\rho_1 = 2\rho_{\text{seed}}$, corresponding to $\rho_2 = \frac{2}{3}\rho_{\text{seed}}$, so that the cell seeding density is higher in the central region, and a second set of simulations in the opposite situation with $\rho_1 = 0.5\rho_{\text{seed}}$, corresponding to $\rho_2 = \frac{5}{4}\rho_{\text{seed}}$. In Fig. 11, we represent the 3D surf plot of the biomass volume fraction at $t = 7, 30, 90$ days of culture, from bottom to top, respectively, for the case $\rho_1 = 2\rho_{\text{seed}}$, while in Fig. 12, we represent the results in the case $\rho_1 = 0.5\rho_{\text{seed}}$. In both conditions, after an initial transient, the distribution of the biomass volume fraction tends to become homogeneous over the domain, because of the greater availability of nutrient in the scaffold

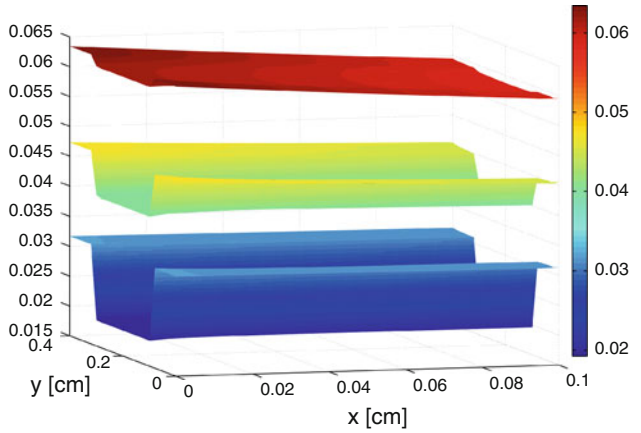

Fig. 12 Spatial distribution of the biomass volume fraction at $t = 7, 30, 90$ days of culture (from *bottom* to *top*) under nonuniform seeding conditions. The seeding density in the inner region is 0.5 times lower than the seeding density in the uniform seeding case

regions less densely seeded, which in turn promotes biomass growth.

5 Discussion and conclusions

The aim of this work was to set up a multiphysics/multiscale computational model for the simulation of the process of biomass growth in an engineered cartilaginous construct, cultured under interstitial perfusion in a bioreactor. The model comprises three phases: cells and ECM (treated as a single phase, biomass), the culture medium, and the time-invariant scaffold porous structure, and provides a self-consistent coupling among the fluid-dynamical environment, the nutrient delivery and consumption and the biomass growth. Compared to previous pore-scale CFD simulations, this approach allows to keep into account the space-time evolution of the growing biomass at affordable computational costs and to perform simulations for any scaffold pore geometry, regular (for example the idealized scaffold pore structures considered in Boschetti et al. (2006); Lesman et al. (2010)) or irregular (for example the ones obtained from the μCT images of Raimondi et al. (2005)).

Concerning the critical issue of the description of the temporal and spatial evolution of the developing biomass, our approach is based on the fundamental experimental observation that in perfused bioreactors biomass growth is influenced primarily by two factors, oxygen tension and fluid dynamical shears (Schulz and Bader 2007). While the role of oxygen delivery to cells has been extensively investigated in several computational studies (see for example, Galban and Locke 1999a,b; Freed and Vunjak-Novakovic 2000; Galbusera et al. 2007, 2008), considerably less attention has been paid to account for the effect of mechanical stimuli in the prediction of biomass growth. Therefore, in this article, we have focused our analysis on the extension of the Monod growth model proposed in Galban and Locke (1999a,b), in such a way that the coupling of cell behavior and mechanical environment is captured through the introduction of a stress-dependent relation for the specific growth rate. The parameters entering such relation have been calibrated on the experimental data of Raimondi (2006) using a simplified reduced model for which the nutrient and stress distributions are assumed to be constant in time and uniform in space, consistently with the environmental conditions of the early culture times of Raimondi (2006). Our modeled dependence of biomass growth on fluid shears is consistent with experimental observations also from a mechanotransduction view point. In fact, in porous cellular constructs, cell seeding results in the formation of a cell monolayer, initially covering the entire internal pore surface of the scaffold. When the constructs are placed in the bioreactor and cultured under interstitial perfusion, the cells proliferate until confluence, a condition in which there is no space left on the pore surface for the cells to invade. Thus, the cells switch their activity from proliferative to matrix production and a thicker biomass layer is formed, composed by cells and their surrounding ECM. The tissue growth process within the construct basically consists in the thickening of such biomass layer while invading the pore space. Increasing the shear stress level sensed by cells of the biomass peripheral layer—the only cells of the biomass that can directly sense those forces—likely increases their doubling rate, as modeled here, because flow-induced signals introduce essentially a proliferative stimulus in these cells (Silver 2006). In fact, the biomass maintains a thin proliferation layer at the free interface with the culture medium, likely covering all the biomass surface exposed to flow during biomass growth.

In the derivation of the fully coupled model, the VAM is systematically employed to obtain macroscopic equations which keep into account microscopic scale contributions by an appropriate definition of effective parameters, such as hydraulic permeability and nutrient diffusivity. Concerning with the permeability, similarly to what done for the biomass growth model, a calibration procedure is carried out to determine its reference value, in such a way that the range of values attained by the correspondingly computed Darcy stresses are compatible with the pore-scale analysis of Raimondi (2006). This approach allows overcoming a critical issue arising in the comparison between shear stress predictions of microscale versus macroscale approaches (see Cioffi et al. 2006; Chung et al. 2007). As for the effective oxygen diffusivity, a simplified two–phase model comprising a solid phase (scaffold) and a "fluid–equivalent" phase (biomass and perfusion medium) has been considered, so that the theory of Wood et al. (2002) can be applied to the problem at hand to yield a closed expression for the nutrient diffusion coefficient.

An extensive numerical validation of the above described computational model has been carried out. Our results can be directly compared to those obtained in Chung et al. (2007), even if in this reference the effect of the shear stress in the growth model as well as of the presence of the scaffold volume fraction in the calculations of the permeability were not considered. The computed increase in biomass volume fraction with culture time is in good qualitative agreement with published data from perfusion experiments (Davisson et al. 2002; Freyria et al. 2005; Mahmoudifar and Doran 2005). Only qualitative agreement may be expected in this regard, because the flow rates, scaffold materials, cell densities and culture medium compositions differ among the various studies. Also, most bioreactor studies are based on the comparison, at the end of cultivation, of constructs subjected to perfused versus nonperfused conditions.

The test case of nonuniform seeding is included to study a situation which tipically arises in perfusion-based bioreactors. As a matter of fact in static culture conditions, cells tend to form a proliferation layer surrounding the cellular construct, likely related to the simultaneous presence, at the construct periphery, of free space for the cells to invade, combined to physiologic oxygenation and catabolite removal. This tendency is not observed in constructs perfused interstitially, as modeled here, due to the beneficial effect of convective transport in maintaining physiologic conditions also at the internal areas of the construct. Hence, in constructs perfused interstitially, the cell proliferation layer extends inside the construct and covers all the biomass surface exposed to flow. However, there exist technical limitations in the cell seeding protocols, which often result in an inhomogeneous initial cell density. The simulation of inhomogeneous seeding patterns, as the ones modeled here, may provide useful information to guide experimentation and to interpret relevant results in these cases.

Future developments will include a 3D implementation of the model, a more thorough investigation of the biomass growth model, featuring independent balance equations for the cellular and the extracellular fractions, and the development of new experimental protocols to be interfaced to the numerical simulations. Transport of solutes other than oxygen can be easily added due to the modular structure of the simulation tool.

6 Appendix

6.1 Parameters of biomass growth model

Not all the parameters entering the right hand side of Eq. 2 are directly available from measurements. In particular, we discuss here the choice of the quantities k_s and r_d. As for r_d, we used the inverse of a lifespan of 30 days, as proposed in Chung et al. (2007). Such value agrees with the experimental data reported in Table 1 of Zhou et al. (2008). Then, we used the equilibrium condition to evaluate the half saturation constant k_s, with $c = c_0$, $\tau = 0$ and $\varepsilon_b = \varepsilon_{b,0}$.

6.2 Solution algorithm and numerical approximation

Let N be the number of time subdivisions of the culture time interval $[0, T]$, $\Delta t = T/N$ the time step and $t^k = k\Delta t$ the k-th time level, $k = 0, \ldots, N$. Then, the solution of the time–dependent nonlinear coupled system (9) is reduced to the solution of a sequence of decoupled linearized sub-problems according to the following block Gauss–Seidel iteration: Given $\varepsilon_b^n = \varepsilon_b(t^n)$, $\mathbf{v}^n = \mathbf{v}(t^n)$ and $c^n = c(t^n)$, for all $n = 0, \ldots, N-1$:

Step 1: solve the Stokes-Brinkman problem

$$\nabla \cdot \mathbf{v}^{n+1} = 0,$$
$$\nabla p^{n+1} = -\mu \varepsilon_f^n K^{-1}(\varepsilon_f^n)\mathbf{v}^{n+1} + \mu \Delta \mathbf{v}^{n+1},$$

and then set $\mathbf{v}(t^{n+1}) = \mathbf{v}^{n+1}$ and $p(t^{n+1}) = p^{n+1}$.

Step 2: solve the nutrient balance equation

$$\nabla \cdot (-D\nabla c^{n+1} + \mathbf{v}^{n+1} c^{n+1}) + R(c^n) = 0,$$

and then set $c(t^{n+1}) = c^{n+1}$.

Step 3: compute the Darcy stress

$$\tau^{n+1} = \frac{\mu |\mathbf{v}^{n+1}|}{\sqrt{K(1 - \varepsilon_s - \varepsilon_b^n)}}$$

and then set $\tau(t^{n+1}) = \tau^{n+1}$.

Step 4: solve the biomass growth equation using a one-step explicit time–marching method

$$\frac{\varepsilon_b^{n+1} - \varepsilon_b^n}{\Delta t} = \Phi_b(\varepsilon_b^n, c^{n+1}, \tau^{n+1}; \Delta t)$$

Φ_b being a suitable increment function, and then set $\varepsilon_b(t^{n+1}) = \varepsilon_b^{n+1}$.

The temporal stability of the above solution algorithm is determined by the appropriate choice of Δt. To this purpose, we first need to study the stability properties of the biomass growth model (2). For this analysis, we assume c and τ to be parameters allowed to vary in the admissible space $\mathcal{P} = (0, c_0] \times [\tau_4, \tau_1]$ and set $f(\varepsilon_b) := r_b \varepsilon_b$. The equation $f(\varepsilon_b) = 0$ has two roots, $\varepsilon_{b,1} = 0$ and

$$\varepsilon_{b,2}(c, \tau) = \frac{c(k_g(\tau) - r_d)}{r_d \rho_b k_s}.$$

It is easy to verify that, since $k_g(\tau) - r_d > 0$ for all $\tau \in [\tau_1, \tau_4]$, $\varepsilon_{b,2} > 0$. To investigate the mathematical nature of

the two equilibrium points, we consider the linearized version of the growth model (2) (Arnold 1973)

$$\frac{d\varepsilon_b}{dt} = \lambda(\varepsilon_\mathrm{b}; c, \tau)\varepsilon_b + g$$

where g is an inhomogeneous term that has no influence on the stability of the problem, and

$$\lambda(\varepsilon_b; c, \tau) := \frac{\partial f}{\partial \varepsilon_b} = \frac{k_\mathrm{g}(\tau)c^2}{(k_\mathrm{s}\rho_\mathrm{b}\varepsilon_b + c)^2} - r_\mathrm{d}. \tag{14}$$

Replacing into the above formula the expressions of the equilibrium points yields $\lambda(\varepsilon_{\mathrm{b},1}; c, \tau) = k_\mathrm{g}(\tau) - r_\mathrm{d} > 0$ for all τ and $\lambda(\varepsilon_{\mathrm{b},2}; c, \tau) = r_\mathrm{d}(r_\mathrm{d} - k_\mathrm{g}(\tau))/k_\mathrm{g}(\tau) < 0$, from which we conclude that $\varepsilon_{\mathrm{b},1}$ is an unstable equilibrium point while $\varepsilon_{\mathrm{b},2}$ is an asymptotically stable equilibrium point. We can now turn to the analysis of the scheme in Step 4, which is the discrete counterpart of problem (2), and we investigate its absolute stability in the sense of Dahlquist (2003). For the ease of presentation, we consider the simplest case of the Forward Euler (FE) method, corresponding to $\Phi_\mathrm{b} = r_\mathrm{b}(\varepsilon_b^n)\varepsilon_b^n$. The study of the sign of λ in (14) reveals that $\lambda < 0$ provided that $\varepsilon_b > \varepsilon_{\mathrm{b,lim}} = c((k_\mathrm{g}(\tau)/r_\mathrm{d})^{1/2} - 1)/(k_\mathrm{s}\rho_\mathrm{b})$, condition that is largely satisfied by the initial value ε_b^0 for every choice of $(c, \tau) \in \mathcal{P}$. In particular, we need to characterize the maximum absolute value of λ. This occurs at $\varepsilon_b = \varepsilon_{\mathrm{b},2}$, in correspondence of $\tau = \tau_1$ and irrespective of the value of the nutrient concentration c. Moreover, setting $\mathcal{I}_\varepsilon = [\varepsilon_{\mathrm{b,lim}}, \varepsilon_{\mathrm{b},2}]$, we have

$$\max_{\substack{\varepsilon_b \in \mathcal{I}_\varepsilon; \\ (c,\tau)\in\mathcal{P}}} |\lambda(\varepsilon_\mathrm{b}; c, \tau)| = r_\mathrm{d}\left(1 - \frac{r_\mathrm{d}}{k_\mathrm{g}(\tau_1)}\right) < r_\mathrm{d} := \lambda_\mathrm{max},$$

so that we can conclude that the FE method in Step 4 is absolutely stable, provided that

$$\Delta t < \frac{2}{\lambda_\mathrm{max}} = 60 \text{ days},$$

which by far exceeds the actual time step used due to accuracy requirements in the simulations. We notice that a similar analysis applies if a higher-order one-step explicit method is used in Step 4, for instance, a 4th-order Runge–Kutta method.

The spatial discretization of each PDE subproblem in the solution algorithm Steps 1–4 is carried out using the Galerkin Finite Element Method (see, e.g., Quarteroni and Valli 1997). In particular, the stable Taylor-Hood pair is used for the approximation of fluid velocity and pressure in Step 1, while piecewise linear elements are used for the approximation of the nutrient concentration in Step 2.

References

Arnold V (1973) Ordinary differential equations. The MIT Press, Cambridge

Bear J (1972) Dynamics of fluids in porous materials. American Elsevier, New York

Boschetti F, Raimondi MT, Migliavacca F, Dubini G (2006) Prediction of the micro-fluid dynamic environment imposed to three-dimensional engineered cell systems in bioreactors. J Biomech 39(3):418–425

Chung C, Chen C, Chen C, Tseng C (2007) Enhancement of cell growth in tissue-engineering constructs under direct perfusion: modeling and simulation. Biotechnol Bioeng 97(6):1603–1616

Cioffi M, Boschetti F, Raimondi MT, Dubini G (2006) Modeling evaluation of the fluid-dynamic microenvironment in tissue-engineered constructs: a micro-CT based model. Biotechnol Bioeng 93(3):500–510

Cioffi M, Kueffer J, Stroebel S, Dubini G, Martin I, Wendt D (2008) Computational evaluation of oxygen and shear stress distributions in 3d perfusion culture systems: macro-scale and micro-structured models. J Biomech 41(14):2918–2925

Contois DE (1959) Kinetics of bacterial growth: relationship between population density and specific growth rate of continuous cultures. J Gen Microbiol 21:40–50

Dahlquist G, Bjorck A (2003) Numerical methods. Dover, New York

Davisson T, Sah R, Ratcliffe A (2002) Perfusion increases cell content and matrix synthesis in chondrocyte three-dimensional cultures. Tissue Eng 8(5):807–816

Dunkelman N, Zimber M, Lebaron R, Pavelec R, Kwan M, Purchio A (1995) Cartilage production by rabbit articular chondrocytes on polyglycolic acid scaffolds in a closed bioreactor system. Biotech Bioeng 46:299–305

Freed L, Vunjak-Novakovic G (2000) Tissue engineering bioreactors. In: Lanza RP, Langer R, Vacanti J (eds) Principles of tissue engineering. Academic Press, San Diego

Freyria AM, Yang Y, Chajra H, Rousseau C, Ronzire MC, Herbage D, Haj AE (2005) Optimization of dynamic culture conditions: effects on biosynthetic activities of chondrocytes grown in collagen sponges. Tissue Eng 11(5–6):674–684

Galban CJ, Locke BR (1999) Analysis of cell growth kinetics and substrate diffusion in a polymer scaffold. Biotechnol Bioeng 65(2):121–132

Galban CJ, Locke BR (1999) Effects of spatial variation of cells and nutrient product concentrations coupled with product inhibition on cell growth in a polymer scaffold. Biotechnol Bioeng 64(6):633–643

Galbusera F, Cioffi M, Raimondi MT (2008) An in silico bioreactor for simulating laboratory experiments in tissue engineering. Biomed Microdevices 10(4):547–554

Galbusera F, Cioffi M, Raimondi MT, Pietrabissa R (2007) Computational modelling of combined cell population dynamics and oxygen transport in engineered tissue subject to interstitial perfusion. Comput Methods Biomech Biomed Engin 10(4):279–287

Grodzinsky A, Levenston M, Jin M, Frank E (2000) Cartilage tissue remodeling in response to mechanical forces. Ann Rev Biomed Engin 2(1):691–713

Guilak F, Hung C (2005) Basic orthopaedic biomechanics and mechano-biology, chap physical regulation of cartilage metabolism. Lippincott Williams and Wilkins, Baltimore 259–300

Haj AJE, Wood MA, Thomas P, Yang Y (2005) Controlling cell biomechanics in orthopaedic tissue engineering and repair. Pathologie Biologie 53(10):581–589

Hsu C, Cheng P (1990) Thermal dispersion in a porous medium. Int J Heat Mass Transfer 33(8):1587–1597

Lemon G, King JR (2007) Multiphase modelling of cell behaviour on artificial scaffolds: effects of nutrient depletion and spatially non-uniform porosity. Math Med Biol 24:57–83

Lesman A, Blinder Y, Levenberg S (2010) Modeling of flow-induced shear stress applied on 3D cellular scaffolds: implications for vascular tissue engineering. Biotechnol Bioeng 105(3):645–654

Mahmoudifar N, Doran P (2005) Tissue engineering of human cartilage and osteochondral composites using recirculation bioreactors. Biomaterials 26:7012–7024

Masaro L, Zhu XX (1999) Physical models of diffusion for polymer solutions, gels and solids. Prog Polym Sci 24:731–775

Maxwell J (1881) Treatise on electricity and magnetism, vol. I. Clarendon Press, Oxford. Reprinted by Dover, New York, 1954

Palsson B, Bhatia S (2004) Tissue engineering, chap. Scaling up for ex vivo cultivation. Pearson Education, London 223–243

Palsson E (2001) A three-dimensional model of cell movement in multicellular systems. Future Gener Comput Syst 17(7): 835–852. doi:10.1016/S0167-739X(00)00062-5

Pazzano D, Mercier K, Moran J, Fong S, DiBiasio D, Rulfs J, Kohles S, Bonassar L (2000) Comparison of chondrogensis in static and perfused bioreactor culture. Biotechnol Prog 16(5):893–896

Quarteroni A, Valli A (1997) Numerical approximation of partial differential equations, 2nd edn. Springer-Verlag, New York

Raimondi M (2006) Engineered tissue as a model to study cell and tissue function from a biophysical perspective. Curr Drug Discov Technol 3(4):245–268

Raimondi M, Boschetti F, Falcone L, Fiore G, Remuzzi A, Marinoni E, Marazzi M, Pietrabissa R (2002) Mechanobiology of engineered cartilage cultured under a quantified fluid-dynamic environment. In: Biomechanics and modeling in mechanobiology, vol 1. Springer-Verlag, Berlin, pp 69–82

Raimondi M, Boschetti F, Falcone L, Migliavacca F, Remuzzi A, Dubini G (2004) The effect of media perfusion on three-dimensional cultures of human chondrocytes: integration of experimental and computational approaches. Biorheology 41(3–4):401–410

Raimondi M, Candiani G, Cabras M, Cioffi M, Laganà K, Moretti M, Pietrabissa R (2008) Engineered cartilage constructs subject to very low regimens of interstitial perfusion. Biorheology 45(3–4):471–479

Raimondi M, Moretti M, Cioffi M, Giordano C, Boschetti F, Laganà K, Pietrabissa R (2006) The effect of hydrodynamic shear on 3d engineered chondrocyte systems subject to direct perfusion. Biorheology 43(3–4):215–222

Raimondi MT, Boschetti F, Migliavacca F, Cioffi M, Dubini G (2005) Micro fluid dynamics in three-dimensional engineered cell systems in bioreactors. In: Ashammakhi N, Reis RL (eds) Topics in tissue engineering, vol 2, chap. 9

Schulz R, Bader A (2007) Cartilage tissue engineering and bioreactor systems for the cultivation and stimulation of chondrocytes. Eur Biophys J 36:539–568

Silver F (2006) Mechanosensing and mechanochemical transduction in extracellular matrix, chap mechanochemical sensing and transduction. Springer, US 211–261

Wang S, Tarbell J (2000) Effect of fluid flow on smooth muscle cells in a 3-dimensional collagen gel model. Arterioscler Thromb Vasc Biol 20(10):2220–2225

Whitaker S (1999) The method of volume averaging. Theory and application of transport in porous media. Kluwer Academic Publishers, Dordrecht

Wood BD, Quintard M, Whitaker S (2002) Calculation of effective diffusivities for biofilms and tissues. Biotech Bioeng 77(5):495–514

Wood BD, Whitaker S (1998) Diffusion and reaction in biofilms. Chem Eng Sci 53:397–425

Zhou P-H, Liu S-Q, Peng H (2008) The effect of hyaluronic acid on IL-1b-induced chondrocyte apoptosis in a rat model of osteoarthritis. Orthop Res 26(12):1643–1648